Applied Catalysis B: Environmental 201 (2017) 182–188

Contents lists available at ScienceDirect

Applied Catalysis B: Environmental

journal homepage: www.elsevier.com/locate/apcatb

Towards an understanding of the beneficial effect of mesoporous materials on the dehydrogenation characteristics of NH_3BH_3

James A. Sullivan*, Rory Herron, Andrew D. Phillips

UCD School of Chemistry, Belfield, Dublin 4, Ireland

ARTICLE INFO

Article history:
Received 17 June 2016
Received in revised form 12 August 2016
Accepted 16 August 2016
Available online 17 August 2016

Keywords:
Ammoniaborane
Hydrogen storage
Mesoporous SiO_2
Reaction mechanism thermal analysis

ABSTRACT

Ammonia borane (AB) was loaded onto a range of mesoporous materials (MCM-41, SBA-15 and MCF) by wet impregnation from THF solutions and its thermal dehydrogenation studied using TGA/MS. The interactions between the AB and the surfaces were characterised using difference FTIR spectroscopy.

The presence of mesoporous materials promotes lower temperature H_2 release, and greater selectivity towards the formation of H_2, i.e. decreased formation of gaseous boron-containing side products. D-FTIR results confirm interactions between isolated silanol groups or surface Si-O-Si species and AB and this supports the proposal that a H-bonding interaction between the surface and deposited AB is important in promoting decomposition at lower temperature. AB interacting with silanol groups decomposes more readily than that coordinated to Si-O-Si.

The effect on the temperature of H_2 release is greater for materials of larger pore size (rather than materials of larger surface area), i.e. MCF > SBA-15 > MCM-41. This suggests that access to the internal surface of the mesoporous material (where the majority of surface silanols are located) is important, and this in turn suggests that polymeric species, which may have restricted access to the internal surface of the different materials, form when AB is dissolved in THF.

Decomposition of B-N-containing gaseous materials (to AB(g)) following their formation, on the silanol groups of the SiO_2, is suggested as the reason for the increased selectivity of the reaction to H_2 (and decreased release of unwanted side products) in the presence of mesoporous material.

1. Introduction

The use of a fuel-cell powered transport fleet in place of the currently used internal combustion-powered vehicles would have several important environmental consequences. These would include a decrease in the emission of localised pollutants, improved fuel economy (as the limitations of the Carnot cycle are bypassed) and (if H_2 fuel was sustainably produced) a decrease in the emission of CO_2 [1]. One of the limitations to the proliferation of H_2-powered Proton Exchange Membrane (PEM) fuel cell vehicles is the H_2 storage problem [2]. Several options for the storage of H_2 have been considered including physical storage using refrigeration [3] and/or high pressure systems [4], physisorption into various media including metal organic frameworks [5] and carbon nanostructures [6], and chemical storage in chemicals such as methanol [7], ammonia [8] or higher hydrocarbons. In the latter the chemical would be reformed to release H_2 on-board a vehicle.

Regarding chemical storage options, the US Department of Energy has stipulated particular mass/volume requirements for the use of chemical H_2 storage materials [9]. Ammonia-borane (AB), NH_3BH_3, meets these requirements. For this reason, the removal of H_2 from AB (either through dehydrogenation or hydrolysis) has recently been extensively studied [10–15].

AB contains 19.5% hydrogen by mass and can release equivalents of H_2 at three different temperatures [16], i.e. 100 °C, 150 °C and at over 900 °C.

Two features of the thermal dehydrogenation of AB militate against its use in the chemical storage of H_2 for use in a PEM fuel cell, i.e. the temperatures required for H_2 release and the generation of gaseous B-N containing side products which act as fuel cell anode catalyst poisons.

Specifically, the first equivalent of H_2 is released at temperatures higher than the optimum operating conditions of a PEM fuel cell, i.e. 70 °C, while the B-N containing gaseous products released include ammonia, borazine, diammonite of diborane (DADB) and molecular $H_4N_2B_2$. As well as acting as fuel cell poisons, the release of these materials into the gas phase hinders any potential for the recycling of the hydrogen storage material.

* Corresponding author.
E-mail address: james.sullivan@ucd.ie (J.A. Sullivan).

http://dx.doi.org/10.1016/j.apcatb.2016.08.040
0926-3373/

The thermal dehydrogenation of AB has been studied [17–22]. One of the major findings of these studies was that AB will dehydrogenate at lower temperatures than reported above if it is held at these temperatures for a significant time. During this "lag" time the H-bonding network holding crystalline AB together is disrupted (generating a so-called AB* phase) and once this happens dehydrogenation proceeds [19].

Furthermore, the presence of mesoporous SiO_2 materials has also been reported to decrease the temperatures required for dehydrogenation and also decrease the concentrations of the undesired gaseous B-N containing fragments which are formed [23–25]. This effect has variously been ascribed to modification of the structural and thermodynamic properties of confined AB.

The current work looks at the effect of varying the porous materials used to promote this effect, and in particular the pore size and the surface characteristics of the materials was studied. The pore size was varied between microporous (zeolitic) materials and mesoporous (MCM-41, SBA-15 and MCF materials) and the surface was varied between a pure SiO_2 material (which contained surface silanol groups) and a material on which the majority of these silanols were removed through condensation with alkyl alkoxy silanes.

The temperatures required for dehydrogenation were monitored using thermogravimetric analysis, while the composition of the evolved gas phase was followed using on-line mass spectrometry. The nature of the interaction between deposited AB and the porous material surface is examined using difference-FTIR.

2. Experimental

The various mesoporous SiO_2 materials used (MCM-41, SBA-15 and MCF) were prepared following the methods reported by Srivastava et al. [26], Cai et al. [27] and Dogu et al. [28] respectively. A C_2H_5-modified MCF sample was prepared using methods described in [29]. (see the Supporting Information document for details).

These mesoporous silicas (MPS) are chemically similar to one another (all being SiO_2) and differ from one another in morpohological and textural areas. Specifically, MCM-41 and SBA-15 are hexagonal mesoporous materials with long channels whose pore sizes range between 2.0 and 6.5 nm (for MCM-41) and 4.6 and 30 nm (for SBA-15). MCM-41 is solely a mesoporous material while, depending on preparation conditions SBA-15 can have both meso and microporosity and in certain cases (depending on wall thickness) the micropores can connect the mesoporous channels. MCF (meso-cellular foam, which condenses around expanded Pluronic 123 micelles) on the other hand does not have an extended mesoporous channel structure but has pore sizes that are generally between 15 and 50 nm. These pores are normally spherical with narrow windows interconnecting each pore. Specific preparation details for each material, as well as for a functionalised MCF material where silanols are removed through condensation with ethyl ethoxy silane, can be found in the Supplementary information document.

N_2 physisorption was carried out on a Quantachrome 4200e instrument and the data were treated to yield BET surface area and BJH pore size measurements. N_2 adsorption desorption profiles from these experiments are shown in Fig. SI 1 in the Supplementary information file.

TGA/MS measurements were performed on a Q500 (TA Instruments) coupled with a HPR20-QIC Atmospheric Gas Analysis System (Hiden Analytical).

AB: mesoporous sample mixtures were prepared by wet impregnation of the solid with THF solutions containing the required masses of AB. In general for these, the required amount of AB was dissolved in the minimum volume of THF. This solution was added drop wise to the support until the support appeared "wet". The support was then dried under vacuum at room temperature and the rest of the solution added in the same manner. When the full solution was added the AB:MPS mixture was dried under vacuum at room temperature for 1 h. No evidence of THF remaining in or on the materials was observed during any of the subsequent TGA/MS experiments. Furthermore, blank experiments in the absence of AB confirmed that no THF remained on the material following vacuum treatment or that any appreciable mass loss from the SiO_2 materials took place at the temperatures of interest in this study (room temperature to 200 °C). This means any mass loss seen during the TGA/MS experiments arose from the decomposition of the deposited AB.

Samples of AB:MCF mixtures with varied mass ratio of 0.5:1 and 2:1 were prepared for analysis. During TGA these mixtures were loaded on an alumina pan enclosed in the furnace under a flow of N_2 (100 mL min^{-1}). The samples were held isothermally at 25 °C for 40 min before their temperatures were raised to 200 °C at a ramp rate of 2 °C min^{-1}. The gas which exited the TGA instrument was analysed using Mass Spectrometry (Hiden HPR-20 QIC). The mass spectrometer was set to scan for masses relating to H_2 ($m/z = 2$), NH_3 ($m/z = 17$), H_2O ($m/z = 18$), AB, borazine ($m/z = 80$), $H_4B_2N_2$ ($m/z = 53$) and diammoniate of diborane (DADB) ($m/z = 62$).

FTIR measurements were carried out on a Vertex 70 FTIR spectrometer equipped with a Globar Infrared source (for a spectral range in the NIR-MIR) and a liquid nitrogen cooled Mercury Cadmium Telluride (MCT) detector. Samples for DRIFT were loaded into a Praying Mantis accessory for analysis. For difference FTIR measurements the background spectrum collected was that of the MPS material and the samples were mixtures of AB:MPS prepared by deposition from THF solutions. Therefore peaks generated were due to the addition of AB (positive peaks in the absorbance spectra), or the removal of surface species on the MPS sample following interaction with AB (negative peaks in the absorbance spectra).

3. Results and discussion

3.1. Textural data

Table 1 shows the BET surface areas of the different MPS materials – along with their pore sizes (as determined by the BJH technique). All values are in the range expected for the different mesoporous materials with the MCM-41 sample having the smallest pores (3.4 nm) and the largest surface area (668 m^2 g^{-1}) and the MCF having the lowest surface area at 217 m^2 g^{-1} and the largest pore sizes (18 nm). The SBA-15 pore size is higher than that of MCM-41 (at 4.3 nm) and also has a surface area intermediate between the other materials (497 m^2 g^{-1}).

3.2. DTGA studies

Fig. SI 2 (a) shows the TGA and DTGA profiles collected during the decomposition of AB under an N_2 flow, while Fig. SI 2 (b) shows the mass spectrometer data collected during the same experiment. These results are in agreement with previously observed data and show that the decomposition takes place in two different steps, one between 85 and 125 °C peaking at 110 °C and the second between

Table 1
Showing textural characteristics of the mesoporous materials and their pore sizes as measured using BET and BJH analysis.

	BET surface area/m^2g^{-1}	Pore size/nm
MCM-41	668	3.4
SBA-15	497	4.3
MCF	217	18

130 and 175 °C peaking at ~160 °C. These are approximately the temperatures at which thermal decomposition of AB is reported to release 1 equivalent (per event) of H_2. Analysis of the exit gas using mass spectrometry shows that H_2 is the major product evolved during the first event, with minor production of borazine, DADB and $H_4B_2N_2$. During the second event significantly more of these B-N containing gaseous species are produced (although with mass spectrometer signals ~2 orders of magnitude lower than that of the evolved H_2). The generation of such amounts of non-selective products mean that any discussion about the numbers of H_2 equivalents released during each event is not meaningful, however we can say that any individual AB formula unit cannot lose more than 2 equivalents of H_2 at temperatures of ~200 °C. In this case however, the sample lost ~46% of its mass (while the loss of 2 equivalents of H_2 would result in a mass loss of ~13.3%). This result mirrors that of Lai [25].

As discussed, this mode of AB decomposition is not useful when application in a PEM fuel cell is considered due to (a) the relatively high temperatures required to release and (b) the production of potential anode catalyst poisons (and the loss of B-N containing material from the residue).

In preliminary experiments a series of TGAs were carried out on AB deposited upon with various commercial ZSM-5 zeolites (Alsi Penta). These had reported pore sizes of ~0.5 nm. The materials varied according to their counter ion (NH_4^+ and Na^+) and their Si/Al ratio (27 and 55). In all cases it was found that the presence of the microporous materials did not influence the decomposition characteristics in terms of either decreasing the temperature required for decomposition/dehydrogenation, or reducing the concentrations of B-N-containing side products detected.

For substantive changes to the temperatures of decomposition and the range of by-products formed mesoporous materials had to be employed.

Fig. 1 shows the DTGA profiles collected from the decomposition of AB:MPS samples (with AB:MPS loadings of 0.5:1) using MCM-41, SBA-15 and MCF as the mesoporous SiO_2 samples. The DTGA profile from the decomposition of AB in the absence of MPS is also shown for comparison. Fig. 2 shows the relevant mass spectrometer profiles from these experiments.

There are two main differences between these reactions and those recorded during the decomposition of AB in the absence of MPS (SI Fig. 2(a)). These are (a) the lower temperatures required for H_2 release (with the two larger-pored MPS) and (b) the much decreased levels of gaseous side products formed when the decomposition takes place in the presence of mespoporous SiO_2 (see Fig. 2, and compare with Fig. SI 2(b)).

Within the data shown in Fig. 1, a trend emerges regarding the effect of the MPS as a function of pore size. The temperatures required for the 1st decomposition of the AB loaded onto MCM-41

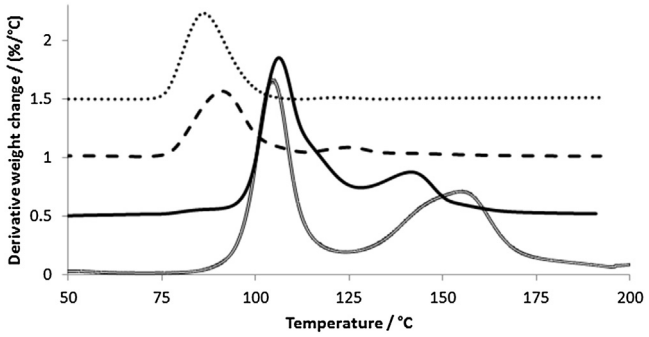

Fig. 1. Displaced DTGA profiles of AB:MPS mixtures with a mass ratio of 0.5 AB:1 MPS. AB-MCM-41 (—), AB-SBA-15 (- -), AB-MCF (. . .). The DTGA profile for pure AB is also shown (=====).

are similar to those seen when AB decomposed in the absence of any mesoporous material, i.e. with decomposition between 95 and 120 °C. The second AB decomposition event over MCM-41 takes place at lower temperatures than was seen when AB alone decomposed, i.e. between 130 and 150 °C, and the mass loss associated with the event is relatively smaller than it had been when AB decomposed on its own, i.e. the DTGA peak is relatively smaller.

When AB decomposition takes place in the presence of the SBA-15 sample the temperature of the first decomposition is decreased to a range between 75 °C and 100 °C and the second decomposition event is also further decreased in terms of both relative mass loss and temperature (taking place between 115 and 130 °C).

Finally, when AB loaded onto MCF mesoporous silica is analysed using DTGA, it can be seen that the temperature of the first decomposition decreased to between 75 and 95 °C (and the associated H_2 evolution is also shows two peaks) while the second decomposition is hardly noticeable in the DTGA profile.

Comparisons of these profiles show that the effects of the presence of MPS are two fold, i.e. the temperature of the first decomposition is decreased (and the extent of the decrease increases with the pore size of the MPS) and the relative importance of the second event decreases (again as the pore size of the MPS increases).

Fig. 2 shows the H_2, AB and borazine mass spectrometer profiles generated from each of these experiments. Borazine was chosen as an example of an undesired side product – it should be noted that there are a range of side products formed – see Fig. SI 2(b). Table 2 shows the maximum temperature of H_2 production for each reaction event.

The mass loss figures from these experiments confirm that significant amounts of gaseous species were lost from the mixtures that were not hydrogen (since only 2 equivalents of H_2 can be released at these temperatures). In terms of overall mass loss the AB:MCF sample lost ~10.8% of its mass (~5 equivalents of H_2), the AB:SBA-5 sample lost ~13.0% (~6 equivalents) and the AB:MCM-41 sample lost ~30.3% of its mass (or 14 H_2 equivalents). Note here we use the term 'equivalents of H_2' as a convenient shorthand to represent mass loss of other material from the mixture.

However, mass spectrometer data (see Fig. 2) shows that none of the gaseous species released were the N-B containing oligomeric species seen when AB decomposed in the absence of SiO_2. In contrast to that situation, there were peaks noted at $m/z = 31$ (see figure) which we have ascribed to AB(g) molecules. This species is not present in the TGA/MS profiles from the decomposition of AB in the absence of any of the mesoporous materials.

It seems that either these side products (e.g. borazine, DADB, $H_4B_2N_2$) are not produced in the presence of the mesoporous material (and the dehydrogenation reaction is selective to the production of AB(g) and H_2), or that they are produced but further decomposed to AB(g) following interaction with the surface. In the former case it may be that the presence of the solid material promotes formation of the AB* phase (see [20]).

Lai et al. [25] also see similar results in complementary TPD experiments, although in their case the side products were not completely eliminated (and in their case there was no tempera-

Table 2
Showing the maximum temperatures of H_2 production during the experiments shown in Fig. 1. Data from decomposition of pure AB(s) is shown for comparison.

	T_{max} (1)/°C	T_{max} (2)/°C	Mass spectrometer profile comments
Pure AB(s)	110	150	H_2 and volatiles – no AB
MCM-41/AB	108	133	H_2 and AB(g)
SBA-15/AB	90	117	H_2 and AB(g)
MCF/AB	80/95	–	H_2 and AB(g)
MCF(C_2H_5)	100	132	H_2, volatiles and AB(g)

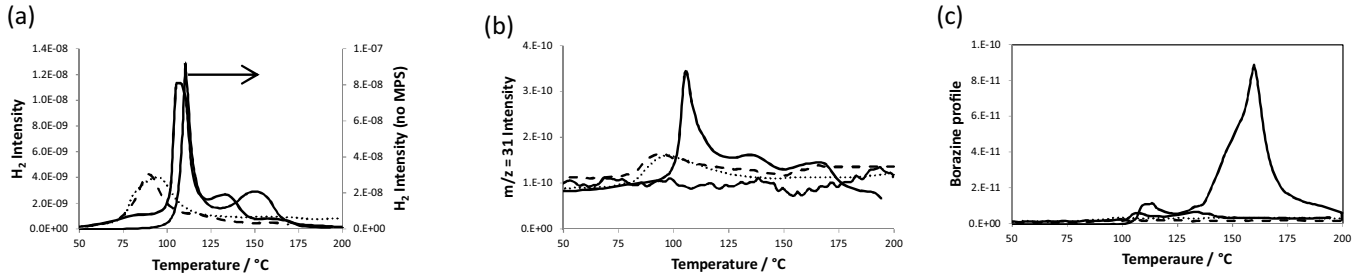

Fig. 2. (a) H_2, (b) AB and (c) borazine mass spectrometer profiles relating to the experiments shown in Fig. 2. AB-MCM-41 (—), AB-SBA-15 (- -), AB-MCF (. . .). Profiles from decomposition of AB in the absence of SiO_2 are also shown (–).

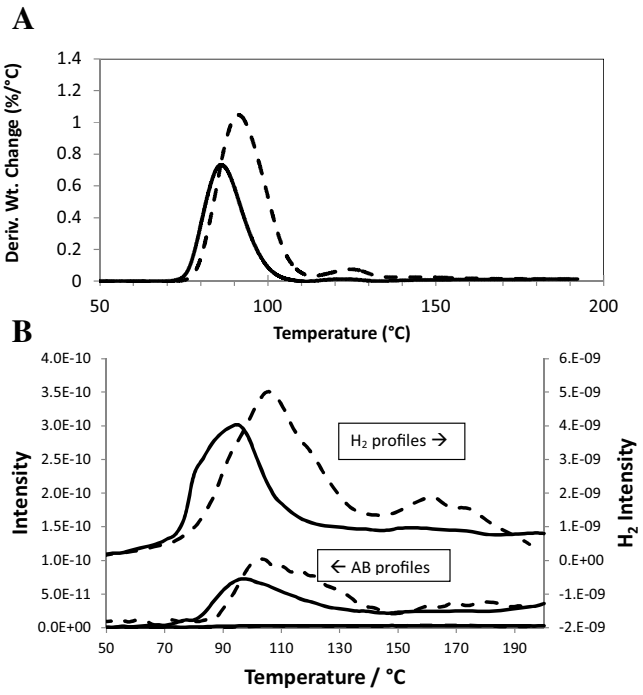

Fig. 3. (a) DTGA of AB:MCF at ratios of 0.5:1 TGA(—) and 2:1. (- -). For comparison, a DTGA of AB in the absence of MCF is in SI Fig 2(a). (b) Mass spectrometer profiles of H_2 (top profiles), AB (middle profiles) and borazine (as a typical oligomeric product, bottom profiles) relating to the experiments shown in Fig. 4. AB:MCF 0.5:1 (—), AB:MCF 2:1 (- -) (profiles from the decomposition of pure AB are shown in Fig SI 2(b)).

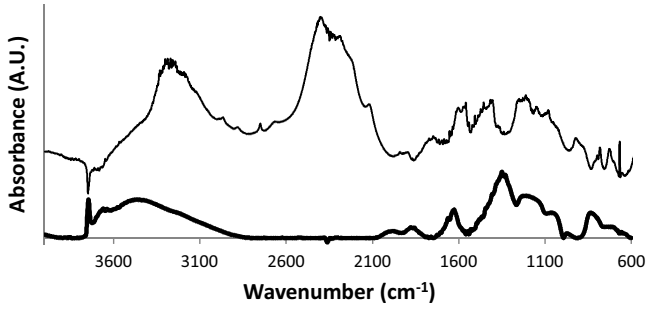

Fig. 4. Difference FTIR spectrum of an AB: MCF mixture. The spectral background was a pure sample of MCF. The lower profile is an FTIR spectrum of MCF.

ture difference between the decompositions in MCM-41 or SBA-15) (Fig. 3).

In attempts to discriminate between these possibilities a series of TGA/MS experiments where the AB:SiO_2 mass ratio was varied was carried out. Fig. 3 shows the results of experiments where the mass of AB is increased fourfold (to a 2:1 AB:MPS mass ratio) on the MCF material. The figure shows that the DTGA profiles change to become composite profiles where a portion of the AB decomposes as was seen in Fig. 1, (i.e. initial decomposition between 70 and 95 °C, with little decomposition at higher temperatures) while the remainder decomposed as was seen in Fig. SI 2 (in the absence of MPS), i.e. initial decomposition between temperatures 90–110 °C with another decomposition between 135 and 170 °C).

We ascribe this to the decomposition of two types of deposited AB, i.e. that deposited in contact with the MCF surface (either internal or external), and (after the surface is saturated with AB) the remainder of the deposited AB crystallizing in no contact with the surface. The latter AB had no interaction with the MCF, and therefore did not experience any beneficial effect (in terms of reduction of the dehydrogenation temperature) during the TGA experiment.

Similar effects were seen with the other two MPS materials as AB mass loading was increased (results not shown).

However, what is more noteworthy about these experiments is the composition of the resultant product stream. Even though in all cases a significant fraction of the AB decomposed as if it were not in contact with the mesoporous material (as determined from the temperatures of decomposition), the concentrations of gaseous side products produced during the experiments were much altered relative to those seen during AB decomposition in the absence of MCF Fig. SI 2(b)). Again, in the presence of MCF only H_2 and gaseous AB(g) are noted irrespective of the temperature of the decomposition of deposited AB (see Fig. 4b). This differs from the situation where AB decomposes in the absence of a mesoporous material where a range of side products including borazine, DADB, NH_3 and $H_4B_2N_2$ were seen (see Fig. SI 2(b)). So, even though the material decomposes at temperatures where it is clear the presence of the mesoporous material has no effect on the decomposition (and thus side products would be expected), the range of side products released is much affected by the presence of the MPS.

This suggests that the decreases in the formation of borazine, DADB and $H_4B_2N_2$ are caused by their decomposition on the SiO_2 before they exit the MPS/AB.

In conclusion, it seems that at low loadings of deposited AB the temperature of decomposition is lowered and the product distribution is much more favourable (generating H_2 and AB(g) rather than a range of B-N containing gaseous species). The former effect is more noticeable for the wider pored materials than for the narrower pored ones (and a trend is evident where the effect is correlated with pore size and not correlated with surface area). This suggests that AB dissolved in THF forms extended linked AB species which cannot access the internal surface of the smaller pored MPS materials (notwithstanding the fact that these are considerably larger than dissolved molecular AB). We have noted a similar unexpected effect following the wet impregnation of group II oxide precursors on different mesoporous materials [30].

The second effect (the beneficial product distribution) suggests that the undesired gaseous fragments of AB oligomers decompose

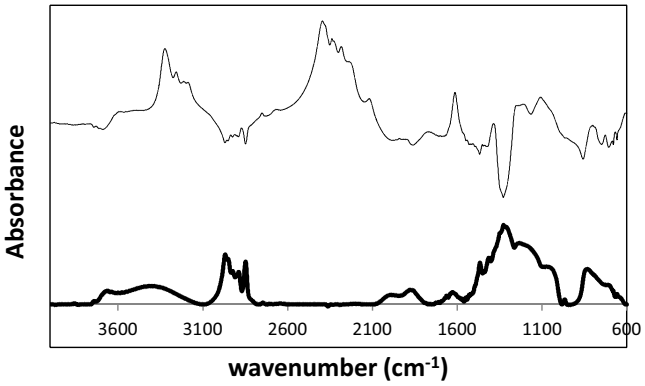

Fig. 5. FTIR Spectrum of C_2H_5-modified MCF (lower profile) and D-FTIR spectrum of AB adsorbed onto this material (upper profile) – note the negative peak at 1345 cm^{-1}.

upon interaction with the mesoporous silica materials to form molecular AB(g).

3.3. FTIR studies

In an attempt to monitor the interactions between the AB and the mesoporous SiO_2 materials a difference FTIR experiment was carried out on the AB:MCF mixture.

Fig. 4 shows the difference FTIR spectrum collected when AB was loaded onto a sample of MCF (at an AB:MCF ratio of 0.5:1). In collecting this spectrum, a sample of pure MCF was used as the background so absorbance peaks pointing up are generated by the deposited AB while those pointing down represent spectral features of the MCF that have been removed following interaction with AB.

This difference spectrum shows a sharp negative peak at 3750 cm^{-1}, which aligns with a peak in the MCF spectrum that is assigned to the vibration of isolated silanol groups. This would indicate an interaction between these groups on the silica and the AB. Given the nature of the group, this is most likely a H-bonding interaction. The other wide bands in the spectrum (3000–3500 cm^{-1} and 2100–2500 cm^{-1}) align with N—H and B—H bands in the spectrum of AB and thus, as expected, show positive absorbances.

There is no evidence for the generation of an Si—O—B band in the difference spectrum (which should appear at approximately 900 cm^{-1} if the OH coordination to the AB was to the boron component of the AB. The absence of a peak in this region may suggest the coordination with the surface is through the N group.

3.4. Experiments using AB:MCF-(C_2H_5)

In order to further probe the interaction between AB and the surface, and specifically the importance of the surface silanol groups to the interaction (and reaction), a sample of MCF from which the surface silanol groups had been removed (following condensation with ethyl triethoxysilane) was prepared. This material is designated as MCF-(C_2H_5) and was characterised before use using FTIR to confirm (a) the removal of the isolated silanol groups and (b) the incorporation of alkyl groups to the surface (see Fig. 5). A mixture of this nanocomposite material with AB (in the same mass ratio as was used above) was then studied using DFTIR and TGA.

The difference FTIR spectrum of this material when in contact with ammoniaborane (using the MCF-(C_2H_5) sample as the spectral background) is shown in Fig. 6. There is no negative peak at 3750 cm^{-1} in this profile showing there is no significant interaction between the AB and surface silanol groups (which is unsurprising since the vast majority of the latter have been removed and replaced with C_2H_5 groups). There are again positive peaks relating to B-H and N-H vibrations in the difference spectrum and there is also a negative peak at 1345 cm^{-1}.

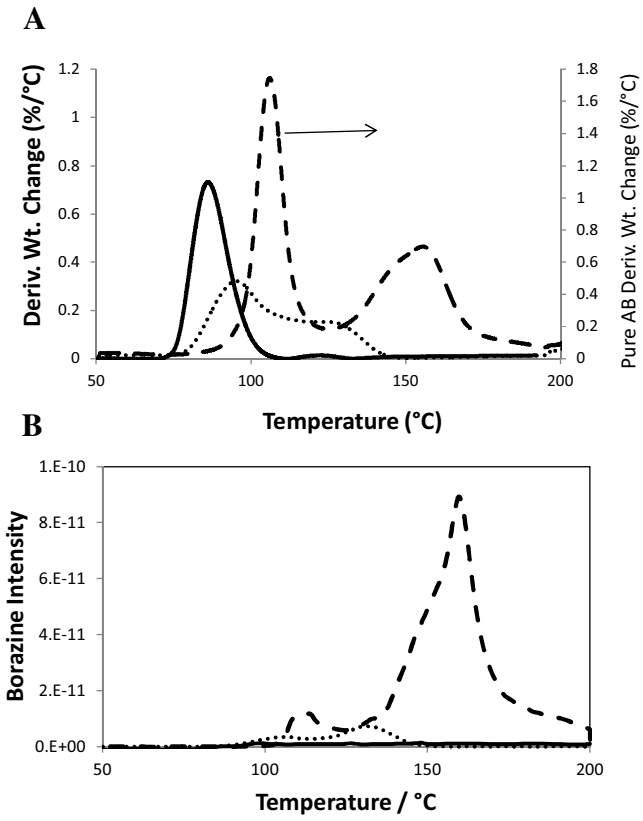

Fig. 6. (a) DTGA profiles for AB (- -), secondary axis, AB:MCF—) and AB:C_2H_5-MCF(. . .). (b) Borazine mass spectrometer profiles relating to the experiments shown in Fig. 6a . AB (- -), AB:MCF (—) and AB:C_2H_5-MCF(. . .).

This latter peak indicates an interaction between the AB species and the surface. Bands in this region of the spectrum have previously been assigned to Si—O—Si stretches in the MCF sample [31] and this result suggests and interaction between the deposited AB and these species. Lai et al. have discussed this interaction in terms of a Lewis base interaction between the SiO_2 scaffold and AB [25].

It was confirmed that the modified material itself was unaffected by TGA at the temperatures used here, so any mass loss seen during these experiments derives from reactions of the deposited AB.

The DTGA profile for the decomposition of AB adsorbed on this material (in a 0.5AB:1MCF-(C_2H_5) loading) is shown in Fig. 6(a), with the DTGA profiles from experiments using pure AB and AB deposited onto unmodified MCF shown for comparison.

It is clear that the removal of the silanol groups has detrimentally affected the ability of the MCF to promote the lower temperature dehydrogenation reaction. Instead of a dehydrogenation event peaking at 86 °C (as was the case when MCF was used to promote the reaction), the event peaks at a temperature of ~96 °C. Having said this, the dehydrogenation reaction still proceeds at lower temperature than it did in the absence of MCF (where the first reaction event peaked at ~110 °C – see Fig. SI 2).

Furthermore, there again appears to be two distinct reaction events (resembling the reaction in the absence of MCF) with the second peaking at ~128 °C (in the absence of MCF this peaked at ~168 °C), while in the presence of unmodified MCF there was only one reaction event (centred at ~86 °C).

Fig. 6(b) shows the production of the borazine (as an example of an unwanted side-product) from the decomposition of AB over the

C_2H_5 modified MCF sample. The borazine profiles from AB decomposition in the absence of MCF are also shown for comparison.

It is clear that the production of this unwanted side product is more noticeable when decomposition takes place in the presence of the modified MCF material than it is in the presence of unmodified MCF (where none were generated). These are however generated at significantly lower concentrations than they were during the AB decomposition in the absence of any mesoporous SiO_2.

In conclusion, when the silanol OH groups are removed from the MCF material, the interaction that had been between AB and these silanol groups is replaced by an interaction between AB and surface Si-O-Si species.

This results in the beneficial effect of the MCF in terms of lowering the temperature required for AB dehydrogenation being lessened. If the interaction (mentioned above as being like a Lewis base interaction) causes disruption of the H-bonding network in AB (leading to a lower temperature decomposition). It is clear that the silanol:AB interaction is a more beneficial hydrogen bonding disruption interaction than the Si-O-Si:AB interaction.

We propose that a H-bonding interaction between deposited NH_3BH_3 species and the silanol groups on the SiO_2 surface promotes the lower temperature dehydrogenation (through the disruption of the H-bonding network in AB) [32]. If this interaction is unavailable (either because the silanol OH groups are inaccessible or have been removed through reaction) another interaction (with the surface Si-O-Si species) can also disrupt the H-bonding network and this also promotes a lower temperature dehydrogenation (but not as effectively as the silanol interaction).

In the presence of the mesoporous SiO_2 samples the concentrations of unwanted side products is much decreased (even in the case where there is little effect on the actual temperatures required for decomposition). Molecular AB(g) is noted in these cases instead. We assume this is from the decomposition of the undesired fragments (borazine etc.) over the silanol goups following their production. Molecular AB is not noted during decomposition in the absence of MPS. This provides a rationale for their presence in the final decomposition studied (where the silanol group concentration had been much reduced by surface condensation with ethyl ethoxy silane).

4. Conclusions

We have shown that the presence of mesoporous SiO_2 can change the thermal decomposition characteristics of ammonia borane in two ways.

Firstly, the temperature of decomposition is decreased in the presence of MPS and, at relatively high loadings of AB, the effect is more noticeable for larger-pored materials. This is the case even when relatively large pored materials (with pore sizes significantly higher than the size of an AB molecule) are considered. This suggests that, under the conditions of our experiments – where THF was the solvent, AB dissolves and deposits to form extended linked AB species which cannot access the internal surface of MCM-41, but have no difficulty accessing the internal surface of MCF materials.

Difference FTIR has shown that the interaction between the MCF materials and wet impregnated AB is through the silanol groups of the surface (suggesting a H-bonding interaction that disrupts the AB lattice).

Deposited AB needs to be activated prior to low temperature decomposition and this involves the formation of the reported AB* phase (in which H bonding between AB molecules is disrupted). H-bonding interactions with silanol groups appears to accomplish this. Si-O-Si surface species may also be able to become involved in disruption of H bonding (albeit more weakly) and there is evidence that this also happens when silanol groups are removed (and indeed the observed effects are weaker).

Secondly, the formation of undesirable B-N containing products is supressed in the presence of SiO_2. This is the case even when the beneficial temperature effect mentioned above is not operating (as the decomposing AB is not in contact with the SiO_2 surface). This effect is independent of the pore size of the MPS material.

Both beneficial effects are decreased (but not eliminated) when surface silanol groups are removed through condensation with alkyl groups. D-FTIR suggests a less valuable (in terms of both decreasing temperature of decomposition and decomposition of unwanted side products) interaction between the deposited AB and Si-O-Si surface species takes place under these conditions.

Future work will study the effect of changing the H-bonding characteristics of the surface (through condensation of different functional groups) to determine whether the decomposition can be further enhanced, and also the effect of changing the solvent for the wet impregnation of AB to determine whether the pore size effect can be bypassed (through solubilisation to smaller linked AB species or to molecular AB). We might expect solvents which can efficiently disrupt the H-bonding network in AB(s) to more effectively solubilise the AB(s) and remove this effect.

Acknowledgement

We acknowledge and thank Science Foundation Ireland for their funding of the Strategic Research Cluster Programme (07/SRC/B1160)

Appendix A. Supplementary data

Supplementary data associated with this article can be found, in the online version, at http://dx.doi.org/10.1016/j.apcatb.2016.08.040.

References

[1] J.J. Spivey, Catal. Today 100 (1–2) (2005) 171–180.
[2] Zhou Li, Renew. Sustain. Energy Rev. 9 (4) (2005) 395–408.
[3] S.M. Aceves, F. Espinosa-Loza, E. Ledesma-Orozco, T.O. Ross, A.H. Weisberg, T.C. Brunner, O. Kircher, Int. J. Hydrogen Energy 35 (3) (2010) 1219–1226.
[4] T.Q. Hua, R.K. Ahluwalia, J.-K. Peng, M. Kromer, S. Lasher, K. McKenney, K. Law, J. Sinha, Int. J. Hydrogen Energy 36 (4) (2011) 3037–3049.
[5] A.G. Wong-Foy, A.J. Matzger, O.M. Yaghi, J. Am. Chem. Soc. 128 (11) (2006) 3494–3495.
[6] T. Yildirim, S. Ciraci,Phys. Rev. Lett. 94 (17) (2005), 175501.
[7] C.S. Song, Catal. Today 77 (1–2) (2001) 17–49.
[8] T.V. Choudhary, C. Sivadinarayana, D.W. Goodman, Catal. Lett. 72 (3–4) (2001) 197–201.
[9] S. Satyapal, J. Petrovic, C. Read, G. Thomas, G. Ordaz, Catal. Today 120 (3–4) (2007) 246–256.
[10] C. Reller, F.O.R.L. Mertens, Angew. Chem. Int. Ed. 51 (2012) 11731–11735.
[11] J.F. Kostka, R. Schellenberg, F. Baitalow, T. Smolinka, F. Mertens, Eur. J. Inorg. Chem. 1 (2012) 49–54.
[12] S. Hausdorf, F. Baitalow, G. Wolf, F.O.R.L. Mertens, Int. J. Hydrogen Energy 33 (2008) 608–614.
[13] P.M. Zimmerman, P. Ankan, C.B. Musgrave, Inorg. Chem. 48 (2009) 5418–5433.
[14] W.R. Nutt, M.L. McKeeb, Inorg. Chem. 46 (2007) 7633–7645.
[15] D.F. Schreiber, C. O'Connor, C. Grave, Y. Ortin, H. Muller-Bunz, A.D. Phillips, ACS Catal. 2 (2012) 2505–2511.
[16] R. Komm, R.A. Geanangel, R. Liepins, Inorg. Chem. 22 (11) (1983) 1684–1686.
[17] M.J. Valero-Pedraza, V. Gascon, M.A. Carreon, F. Leardini, J.R. Ares, A. Martin, M. Sanchez-Sanchez, M.A. Banares, Microporous Mesoporous Mater. 226 (2016) 454–465.
[18] W.J. Shaw, J.C. Linehan, N.K. Szymczak, D.J. Heldebrant, C. Yonker, D.M. Camaioni, R.T. Baker, T. Autrey, Angew. Chem. Int. Ed. Engl. 47 (39) (2008) 7493–7496.
[19] F.H. Stephens, V. Pons, R. Tom Baker, Dalton Trans. 25 (2007) 2613–2626.
[20] G. Wolf, J. Baumann, F. Baitalow, F.P. Hoffmann, Thermochim. Acta 343 (2000) 19–25.
[21] F. Baitalow, J. Baumann, G. Wolf, K. Jaenicke-Röbler, G. Leitner, Thermochim. Acta 391 (2002) 159–168.
[22] J. Baumann, F. Baitalow, G. Wolf, Thermochim. Acta 430 (2005) 9–14.
[23] A. Gutowska, L. Li, Y. Shin, C.M. Wang, X.S. Li, J.C. Linehan, R.S. Smith, B.D. Kay, B. Schmid, W. Shaw, M. Gutowski, T. Autrey, Angew. Chem. Int. Ed. Engl. 44 (23) (2005) 3578–3582.

[24] T.K. Nielsen, K. Manickam, M. Hirscher, F. Besenbacher, T.R. Jensen, Nanoscale 3 (2011) 2086–2098.
[25] S.-W. Lai, H.-L. Lin, T.L. Yu, L.-P. Lee, B.-J. Weng, Int. J. Hydrogen Energy 37 (2012) 14393–14404.
[26] R. Srivastava, D. Srinivas, P. Ratnasamy, Microporous Mesoporous Mater. 90 (1–3) (2006) 314–326.
[27] Q. Cai, W.-Y. Lin, F.-S. Xiao, W.-Q. Pang, X.-H. Chen, B.-S. Zou, Microporous Mesoporous Mat. 32 (1–2) (1999) 1–15.
[28] O. Aktas, S. Yasyerli, G. Dogu, T. Dogu, Mater. Chem. Phys. 131 (1–2) (2011) 151–159.
[29] J.A. Sullivan, L. Sherry, Catal. Today 175 (2011) 471–476.
[30] J.A. Sullivan, L. Sherry, Catal. Commun. 60 (2015) 88–91.
[31] X. Wang, K.S.K. Lin, J.C.C. Chan, S.J. Cheng, Phys. Chem. B 109 (5) (2005) 1763–1769.
[32] W.J. Shaw, M. Bowden, A. Karkamkar, C.J. Howard, D.J. Heldebrant, N.J. Hess, J.C. Linehan, T. Autrey, Energy Environ. Sci. 3 (6) (2010) 796.